ACS APPLIED ENERGY MATERIALS
Cite This: ACS Appl. Energy Mater. 2019, 2, 1380−1387
Article
www.acsaem.org

Development of New Bifunctional Dense Ceramic-Carbonate Membrane Reactors for Gas Mixtures Separation, through CO Oxidation and Subsequent CO_2 Permeation

Oscar Ovalle-Encinia, Pedro Sánchez-Camacho, Daniela González-Varela, and Heriberto Pfeiffer*

Laboratorio de Fisicoquímica y Reactividad de Superficies (LaFReS), Instituto de Investigaciones en Materiales, Universidad Nacional Autónoma de México, Circuito exterior s/n, Cd Univeritaria, Del. Coyoacán, CP 04510, Ciudad de México, Mexico

ABSTRACT: This work presents a dense ceramic-carbonate membrane as a new kind of reactor, where CO oxidation and CO_2 permeation processes are subsequently produced. This kind of membrane reactors may be applied for hydrogen enrichment of syngas mixtures. In here, a composite (doped-ceria and perovskite) was synthesized, sintered, and infiltrated with molten carbonates, showing that the reactor is able to perform both processes: the CO oxidation at the membrane reactor surface and subsequent CO_2 permeation through the molten carbonate phase. Moreover, results evidenced that perovskite phase importantly improves the oxygen permeation from the sweep to feed side (inverse permeation), enhancing CO oxidation and CO_3^{2-} formation without releasing oxygen on the feed side. When oxidation-permeation test was evaluated on a synthetic syngas mixture (H_2 + CO), it was observed that this membrane reactor has an important selectivity for CO oxidation, over hydrogen oxidation, confirming the possible use of this kind of membrane reactors for hydrogen enrichment in different applications.

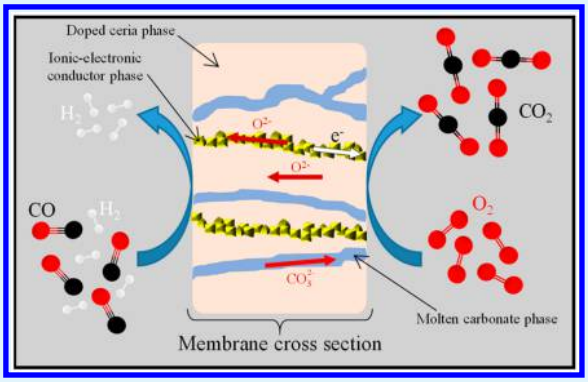

KEYWORDS: *CO oxidation, CO_2 permeation, ceramic dense membrane, ionic conduction, membrane reactor, molten carbonate*

INTRODUCTION

Gas-separation processes have become one of the most promising strategies for different industrial applications with carbon oxide (CO and CO_2) separation among them.[1,2] Within this context, syngas comprises hydrogen and carbon oxides and is usually produced and used at high temperatures.[3] Therefore, H_2 enrichment through catalytic processes, such as carbon oxide oxidation, and different separation mechanisms at high temperatures are of great interest[4−14] for different applications where pure hydrogen may be used as a clean energetic vector.[15]

In the case of CO_2, different membrane systems have been developed, including materials such as zeolites, polymers, ceramics, and different molecular sieves.[11,16,17] Specifically, the so-called dense dual-phase membranes have shown highly interesting CO_2 separation properties at high temperatures.[18] These membranes comprise a porous solid support infiltrated with molten carbonates. Ceramic supports must ideally have oxygen ionic and electronic conductive properties to facilitate different conduction processes, such as oxygen anion conduction from the sweep to feed membrane sides (oxygen inverse permeation).[18−23] It has been proposed that CO_2 permeation on ceramic-carbonate membranes is performed by the reaction of oxygen ions from the ceramic oxide with CO_2 present on the upstream side, thus producing carbonate ions that diffuse through the molten carbonate phase because of CO_2 partial pressure gradients between both sides of the membrane. The CO_2 is desorbed on the downstream side through a reversible decarbonation process and swept from the surface. Oxygen ions are reincorporated and diffused on the ceramic phase as a consequence of decarbonation. Additionally, because oxygen conduction appears to be one important step in the overall CO_2 permeation mechanism, the incorporation of different perovskites into dense ceramic-carbonate membranes has been tested because these materials present good ionic-electronic conduction properties, whereas doped-ceria materials only present ionic conduction.[20,22,23] For example, Zhu et al.[24] as well as Ovalle-Encinia et al.[20] have reported good O_2 and CO_2 permeations, respectively, by using different doped-ceria based membranes mixed with the $Sm_{0.6}Sr_{0.4}Al_{0.3}Fe_{0.7}O_3$ perovskite phase, where this perovskite increases the oxygen conduction because of the large amounts of anion vacancies on its crystalline structure. Nevertheless, it must be pointed out that there is not any membrane report on literature directly related to the CO sorption and subsequent permeation on ceramic membrane systems.

High-temperature ceramic membrane reactors have been proposed for hydrogen production, using different reforming reactions.[25,26] This kind of membrane reactor has the potential to become a disruptive new technology for different industrial

Received: November 12, 2018
Accepted: January 30, 2019
Published: January 30, 2019

DOI: 10.1021/acsaem.8b01947
ACS Appl. Energy Mater. 2019, 2, 1380−1387

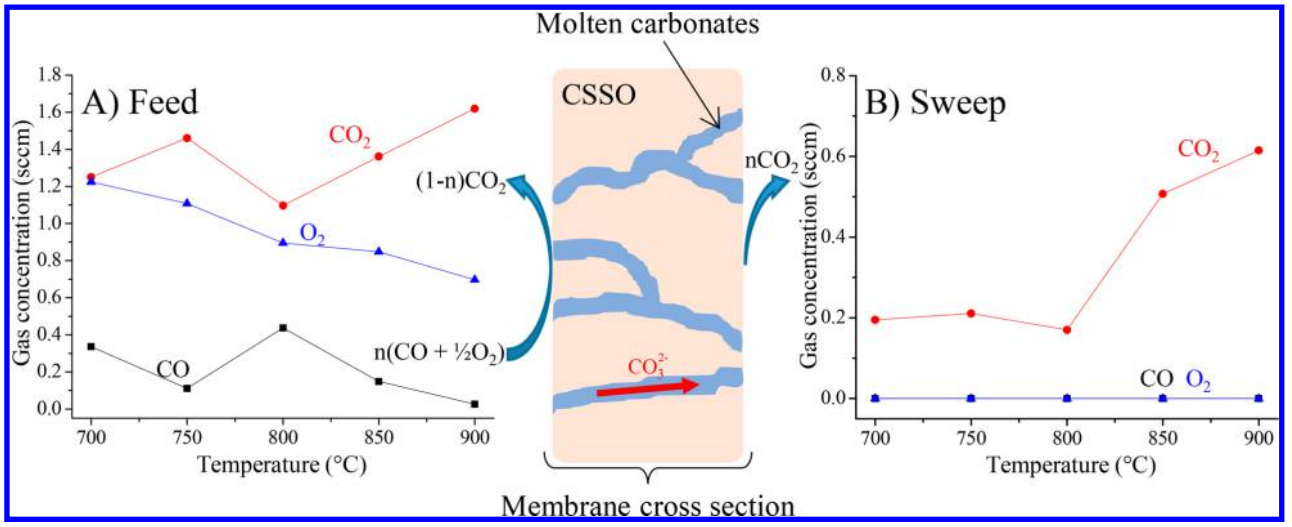

Figure 1. Schematic representation of CO oxidation and CO_2 permeation processes on a CSSO-molten carbonate dense membrane reactor (center) and gas compositions on feed (A) and sweep (B) sides as a function of temperature.

processes performed at high temperatures. For example, a catalytic-free membrane was able to convert CO and H_2O to H_2 and CO_2, removing CO_2 at $T > 800$ °C.[25] Hence, dense ceramic-carbonate membranes can be used in direct CO_2 permeation or multiple processes, including catalytic and permeation steps.

Hydrogen enrichment, coming from syngas mixtures (H_2 + CO), is produced by selective CO oxidation (reaction 1) and subsequent CO_2 permeation. Nevertheless, CO oxidation cannot be produced in the presence of oxygen because it might react with H_2 to produce steam water (reaction 2). Conversely, some reports have shown that H_2 might increase CO oxidation on different materials by different reaction mechanisms.[23,27]

$$CO + \frac{1}{2}O_2 \rightarrow CO_2, \quad \Delta H_{30^\circ C} = -283.0\ \text{kJ/mol} \tag{1}$$

$$H_2 + \frac{1}{2}O_2 \rightarrow H_2O \quad \Delta H_{30^\circ C} = -483.6\ \text{kJ/mol} \tag{2}$$

On the basis of the previous descriptions, the aim of this work was to analyze a Sm−Sr-doped ceria and perovskite composite ($Ce_{0.80}Sm_{0.15}Sr_{0.05}O_{2-\delta}$−$Sm_{0.6}Sr_{0.4}Al_{0.3}Fe_{0.7}O_{3-\delta}$, CSSO−SSAF) in a new possible application as a bifunctional membrane reactor to facilitate CO oxidation and subsequent CO_2 permeation in the presence of hydrogen. Thus, this new kind or membrane reactors would be used for H_2 enrichment on different industrial ant technological applications.

EXPERIMENTAL SECTION

Doped ceria ($Ce_{0.80}Sm_{0.15}Sr_{0.05}O_2$, CSSO) and composite ($Ce_{0.8}Sm_{0.15}Sr_{0.05}O_2$−$Sm_{0.6}Sr_{0.4}Al_{0.3}Fe_{0.7}O_3$, CSSO−SSAF, 77−23 wt %) samples were synthesized via the EDTA−citrate complex method.[20,28,29] The CSSO−SSAF ratio was analyzed and optimized by the amount of oxygen inverse permeation, where it should be maximized without allowing oxygen release in the feed side (data not shown). Each material was mixed with poly(vinyl alcohol) (PVA, 1 wt %) and pressed at 30 MPa using a 30 mm diameter die. The disks were sintered at 1100 °C for 20 h to obtain supports with ∼40% porosity. Finally, dense dual-phase membrane reactors were obtained after support direct infiltration of molten carbonates (Li_2CO_3/Na_2CO_3/K_2CO_3 = 42.5/32.5/25.0 mol %) at 550 °C. Crystalline phases of powders, supports, and membrane reactors were characterized by X-ray diffraction using a diffractometer (Bruker, D8 Advance) with a Cu Kα (1.54059 Å) radiation source operating at 35 kV and 30 mA, where each sample was measured in the 2θ range of 20−120° with a step size of 0.02°. The membrane microstructure was analyzed via field emission scanning electron microscopy and energy dispersive X-ray spectroscopy mapping using a JEOL JSM 7800F (FE-SEM) instrument coupled with an Oxford Instrument X-Max spectrometer. Moreover, the chemical stability of the reactor membrane was analyzed by dynamic and isothermal thermogravimetric analysis (TGA), using different atmospheres. These analyses were accomplished with a Q500HR equipment (TA Instruments). Initially, sample was heat treated with a heating rate of 5 °C/min, from room temperature to 900 °C, under the following gas mixtures: CO_2 (Praxair, grade 3.0), CO (5 vol % N_2 balance, Praxair certificate standard), N_2, (Praxair grade 4.8), O_2 (Praxair grade 3.0), as well as CO−O_2 and CO−O_2−CO_2 gas mixtures. Then, some isothermal analyses were performed between 700 and 900 °C using a CO−O_2 gas mixture to analyze the long-term stability of this sample under an oxidative atmosphere.

The CO oxidation and CO_2 permeation experiments were performed several times between 700 and 900 °C after 30 min of thermal stability, showing high reproducibility. The membrane reactors were sealed into an inner alumina tube (25 mm) using a ceramic sealant paste.[20] Three different gas flow mixtures were used in CO oxidation and subsequent CO_2 permeation experiments: (i) CO/O_2 (3/3 mL/min), (ii) CO (3 mL/min), and (iii) CO/H_2 (3/4 mL/min) on the feed side (upstream) and O_2 (3 mL/min) on the sweep side (downstream), only for the last two feed gas concentrations. For comparison purposes, CO_2 and CO_2−O_2 flows were tested as well on feed side. To obtain a total flux of 100 mL/min, Ar was always used as sweeping gas in the feed and sweep membrane sides. Permeated and nonpermeated gases were analyzed with a GC-2014 gas chromatograph (Shimadzu) equipped with a carboxen-1000 column, which is able to separate CO, CO_2, O_2, and H_2. On the basis of these data, the CO_2 recovery (R_{CO_2}) and CO conversion (X_{CO}) were determined using the eqs 3 and 4, respectively.

$$R_{CO_2} = \frac{F_{CO_2}^{\text{sweep-out}}}{F_{CO_2}^{\text{sweep-out}} + F_{CO_2}^{\text{feed-out}}} \times 100 \tag{3}$$

where $F_{CO_2}^{\text{sweep-out}}$ and $F_{CO_2}^{\text{feed-out}}$ are CO_2 flow rates of sweep-out stream and feed-out stream, respectively.

$$X_{CO} = \frac{F_{CO}^{\text{feed-in}} - F_{CO}^{\text{sweep-out}} - F_{CO}^{\text{feed-out}}}{F_{CO}^{\text{feed-in}}} \times 100 \tag{4}$$

DOI: 10.1021/acsaem.8b01947
ACS Appl. Energy Mater. 2019, 2, 1380−1387

where $F_{CO}^{feed\text{-}in}$, $F_{CO}^{feed\text{-}out}$, and $F_{CO}^{sweep\text{-}out}$ are CO flow rates of feed-in, feed-out, and sweep-out streams, respectively.

Moreover, as this gas chromatograph column is not able to detect water vapor, nonpermeated gases were analyzed by FTIR, only in those cases where H_2 was used on the feed side. The semiquantitative calibration curves were produced by flowing different controlled amounts of CO_2, CO, and $H_2O_{(v)}$. For this analysis, it was used an Alpha Platinum FTIR spectrometer from Bruker connected to a ZnS gas flow cell, which is able to be heated to avoid any possible condensation.

RESULTS AND DISCUSSION

Initially, an oxidation-permeation experiment was performed on a CSSO-carbonate dense membrane reactor, using CO and O_2 ($CO:O_2$ = 1:1, implying an oxygen excess) on the feed membrane side to determine process viability, although real membrane reactors would not use oxygen in the feed side. Figure 1 shows CO oxidation and CO_2 permeation on a CSSO-carbonate dense membrane reactor with CO, CO_2, and O_2 concentrations as a function of temperature. From the feed side, it is evident that CO is only partially oxidized to CO_2. CO concentration decreased, while CO_2 concentration increased, as expected. Indeed, CO conversion increased as a function of temperature, reaching an efficiency of 98.3% at 900 °C. These results are in good agreement with the oxygen consumption increment observed as a function of temperature. On the sweep side, CO and O_2 were not detected, but CO_2 was permeated with a maximum flux of 1.11×10^{-3} mol/m^{2}s, showing a CO_2 recovery of 18.5%, despite the low CO_2 partial pressure on the reaction side. In a similar way than CO oxidation increased as a function of temperature on the feed side, CO_2 permeation increased substantially on the CSSO-carbonate membrane reactor due to temperature.

However, as it was previously mentioned, if this kind of membrane reactor were used in hydrogen enrichment of syngas, oxygen would not be fed on that side of membrane reactor but might be fed from the sweep side. In addition, it must be taken into account the fact that part of the infiltrated carbonates may be released modifying the final carbon mass balance. Something similar can be established for oxygen, which may be taken from CSSO structure for the CO oxidation. Thus, other CSSO ceramic-molten carbonate membrane reactors were tested supplying CO, $CO-O_2$, or CO_2 (3 vol %) on feed side in presence or absence of O_2 on the sweep side. The $CO-O_2$ and CO_2 flows were tested for comparison purposes. Figure 2 shows the CO evolution, on feed side, obtained under all the gas mixtures described above. As it would be expected, the absence of oxygen on feed side importantly decreased the CO oxidation. In presence of oxygen, CO oxidation reached efficiencies as high as 98.3% at 900 °C, independently of the oxygen inverse permeation possibility. On the contrary, when oxygen was only obtained through the CSSO phase, CO oxidation was highly limited to 17−19% of efficiency. Additionally, when oxygen was flow on the sweep side, an slight CO oxidation decrement was observed (in absence and presence of oxygen on feed side). This result must be related to variations on the oxygen diffusion concentration gradient produced by the presence or absence of oxygen on the sweep side. Moreover, when oxygen was not flowed on the sweep side, it was never detected in that membrane side, showing that there was not oxygen release on that membrane side. Hence, these results clearly show that oxygen availability highly controls the CO oxidation and any further CO_2 permeation possibility.

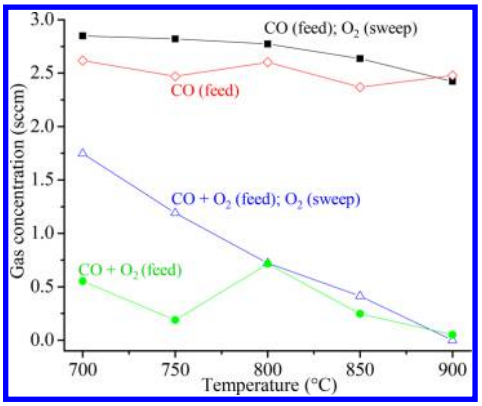

Figure 2. Carbon monoxide concentrations on feed side, varying feed, and sweep gas compositions as a function of temperature on a CSSO-molten carbonate dense membrane reactor.

Figure 3 shows the CO_2 formation and permeation results on feed and sweep sides of the CSSO-carbonate membrane reactor, and they were compared with the observed CO_2 permeation when using a CO_2 (3 vol %) feed gas flow. The CO_2 formation fits well with the CO oxidation values reported above, where the oxygen presence on feed side highly promoted CO_2 formation (Figure 3A). On the contrary, when O_2 was not present on feed side, the CO_2 formation decreased. Nonetheless, it must be pointed out that CO_2 production increased when oxygen was supplied on sweep side, showing that O_2 is been inversely permeated. Moreover, when

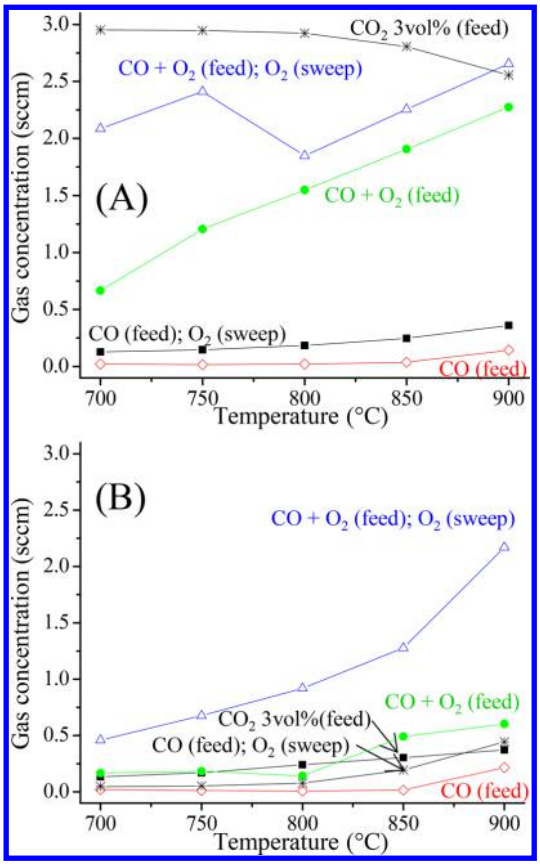

Figure 3. Carbon dioxide concentrations on feed (A) and sweep (B) sides, varying feed and sweep gas compositions, on a CSSO-molten carbonate dense membrane reactor, as a function of temperature.

DOI: 10.1021/acsaem.8b01947
ACS Appl. Energy Mater. 2019, 2, 1380−1387

CO_2 was supplied, its concentration only decreased around 14% at 900 °C, suggesting a low CO_2 permeation efficiency.

As it would be expected, all these membrane reactors presented some CO_2 permeation, although some interesting features that must be pointed out (Figure 3B). The presence of oxygen on sweep side always produced higher CO_2 permeations than those presented in oxygen absence. For example, the CO_2 permeation in a flow of CO + O_2 increased more than 40−50% at any temperature, when O_2 was supplied on sweep side. A similar behavior was observed when only CO was presented on feed side.

Moreover, when CO_2 permeation (using 3 vol % of CO_2 on feed side) is compared with the CO oxidation-permeation results, two aspects must be pointed out (Figure 3B): (i) the amounts of CO_2 permeated were similar for CO_2 or CO initial flows, if O_2 was present on the sweep side, and (ii) the presence of oxygen on feed side (CO + O_2 cases) tended to increase the amounts of CO_2 permeated, in comparison to the CO_2 (3 vol %) case. Thus, the catalytic (CO oxidation) and oxygen inverse permeation processes enhanced the final CO_2 permeation. Hence, it is possible to point out that the CSSO-carbonate dense membrane reactor is able to perform the following processes: (i) CO oxidation at the membrane reactor surface on the feed side, (ii) CO_2 permeation through the molten carbonate phase, and (iii) oxygen permeation from sweep to feed side (inverse permeation) through the CSSO phase. Moreover, oxygen inverse permeation seems to be the limiting step of whole process.

On the basis of these results, a new reactor membrane was prepared by adding a SSAF phase to enhance the oxygen conduction. The CSSO−SSAF composite was corroborated by XRD (data not shown), where both phases were identified as fluorite (43-1002 PDF file) and perovskite (28-1227 PDF file) phases for CSSO and SSAF compounds, respectively. Figure 4 shows the microstructural characterization of CSSO−SSAF support and membrane reactor cross sections. The CSSO−SSAF support cross-section shows a homogeneous macroporous microstructure composed of tiny sintered particles with a size of approximately 200−400 nm (Figure 4A). Once the carbonates were infiltrated (Figure 4B), the macroporosity practically disappeared, and the membrane reactor presented two different contrasts due to carbonates (dark areas) and the CSSO−SSAF support cross-section (bright areas). Homogeneous dispersion of CSSO and SSAF phases was confirmed by EDS elemental mapping (Figure 4C). Sm and Sr were found on both samples, whereas Ce was found only on CSSO, and Al and Fe were found on SSAF. Therefore, the elemental distribution shows homogeneous dispersion of CSSO and SSAF phases. In addition, the alkaline carbonates presented a relatively good dispersion and pore filling, as evidenced by the backscattered image and the Na, K, and C EDS distributions (Li cannot be detected with this technique).

Additionally, dynamic and isothermal thermogravimetric experiments were performed for testing chemical reactivity−stability of this reactor membrane using different atmospheres. Dynamic thermogravimetric data showed a weight increment of around 0.7 wt % from 400 to 700 °C in saturated CO_2, which means a slight chemisorption (Figure 5). In presence of CO, it can be seen a 0.3 wt % increase up to 700 °C, but at 800 °C, a desorption process was produced. In this case, the low CO_2 partial pressure (assuming a partial CO oxidation) in the interface gas−solid produced a decomposition of molten carbonates. Also, this process was observed in the presence of

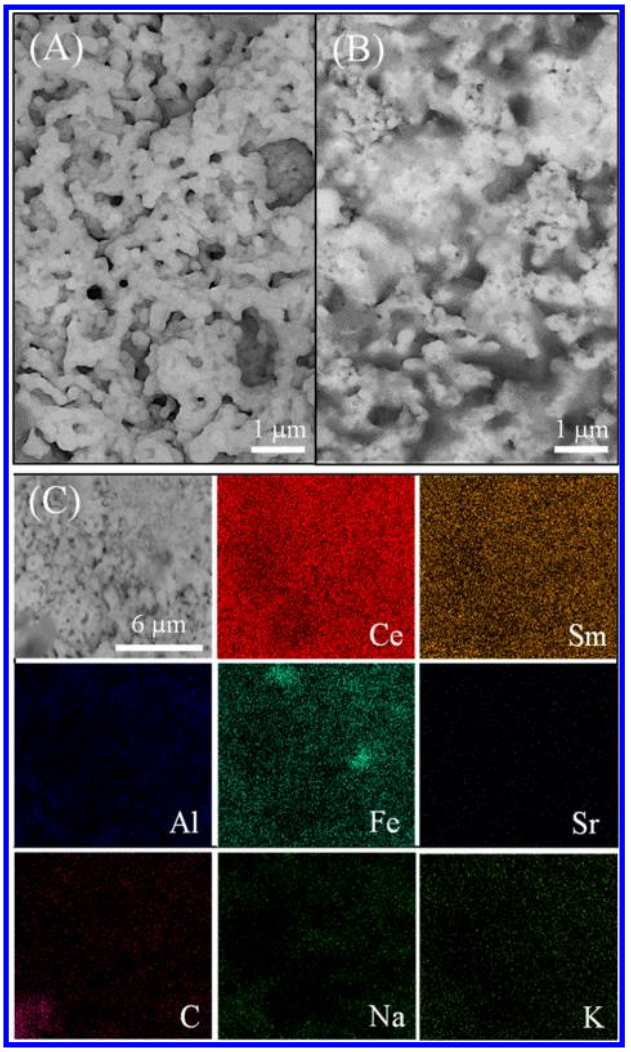

Figure 4. Scanning electron images of different microstructural features of CSSO−SSAF support (A) and molten-carbonate-infiltrated membrane reactor (B) cross sections, as well as secondary image and EDS elemental mapping of the surface membrane reactor (C).

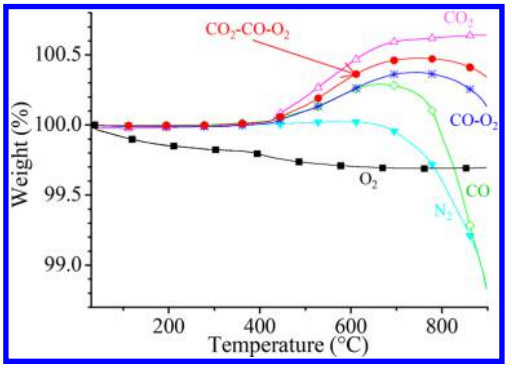

Figure 5. Dynamic thermogravimetric analysis of the CSSO-SSAF-molten carbonate dense membrane reactor using different gases.

N_2, where the weight change was −1.2% at 900 °C. Into an oxidative atmosphere (O_2), a slight weight decrease of −0.3% was observed from 400 to 900 °C. This can be attributed mainly to the carbonates decomposition. In the CO−O_2 and CO−O_2−CO_2 gas mixture systems, it was observed a weight change between 0.3 and 0.4 wt % over 400 °C, while between

DOI: 10.1021/acsaem.8b01947
ACS Appl. Energy Mater. 2019, 2, 1380−1387

700 and 900 °C a desorption process was presented. All these experiments showed a high thermal stability under different chemical environments. Anyhow, as this membrane reactor would be tested under oxidative conditions, different isothermal experiments (700−900 °C) were performed for long times using, specifically, a $CO-O_2$ gas flow (N_2, balanced).

All the $CO-O_2$ isothermal experiments showed a slight loss of weight as a function of time (Figure 6), which are in good

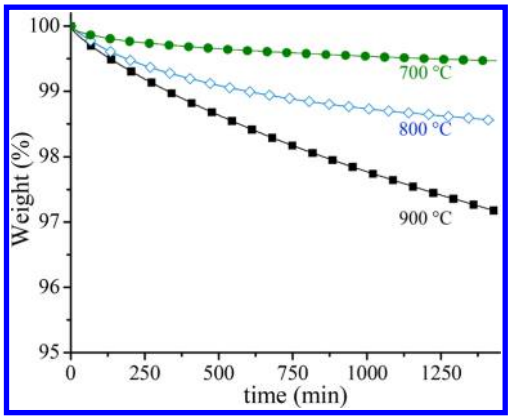

Figure 6. Isothermal thermogravimetric analysis of the CSSO−SSAF−molten carbonate dense membrane reactor at different temperatures (700−900 °C) under $CO-O_2$ (N_2 balance) gas flow.

agreement with the previous dynamic thermograms. At 700 °C, membrane reactor only lost 0.5 wt % after 1400 min. On the contrary, the membrane reactor lost 1.5 and 2.8 wt % at 800 and 900 °C, respectively, after the same test-time. The weight loss observed in these experiments must be attributed to partial molten carbonate decompositions, which increases as a function of temperature. Moreover, the XRD patterns of these isothermal products (data not shown) did not show structural changes of crystalline structures, as the CSSO and SSAF phases were preserved. Therefore, all the weight changes observed by these thermal experiments correspond to chemical transformations produced over the solid−gas interface.

After the membrane reactor characterization, it was evaluated for the CO oxidation and subsequent CO_2 permeation assisted by oxygen inverse permeation, where the correct carbonate impregnation and CSSO−SSAF homogeneity were corroborated. Figure 7 shows that CO oxidation process was produced, confirming that oxygen presented an inverse permeation process. CO oxidation efficiency increased to ∼10−20% of total CO flow, in comparison to previous experiment, where SSAF phase was not present. Of course, this increment must be attributed to oxygen conduction mainly produced on SSAF phase. Moreover, it is evident that CO did not permeate, but CO_2 did, although the CO oxidation process was increased as a function of temperature with a consequent CO_2 permeation increment. In addition, on sweep side, it is observed the presence of oxygen. Thus, only an oxygen fraction presented inverse permeation. In this case, it must be pointed out that oxygen inverse permeation tended to decrease as a function of temperature, which should be related to O_2 adsorption equilibrium changes on the sweep side of the membrane reactor, affecting the CO oxidation process at temperatures higher than 800 °C (see Figure 7A). On the basis of this figure, it can be established that CO oxidation was

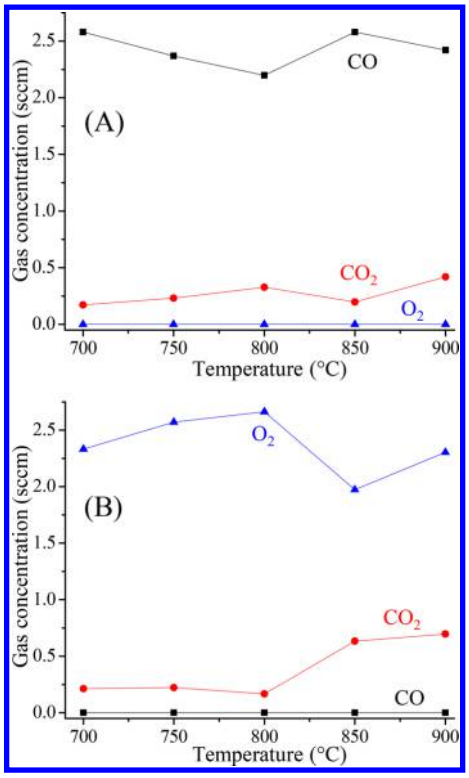

Figure 7. Gas compositions on feed (A) and sweep (B) sides as a function of temperature, on a CSSO−SSAF−molten carbonate dense membrane reactor.

increased as a function of temperature although the oxygen inverse permeation slightly decreased.

Finally, the CSSO−SSAF−molten carbonate membrane reactor was evaluated for the same process, adding H_2 on feed side, to simulate a syngas composition. Thus, CO and H_2 were supplied on feed side, while O_2 was fed on sweep side. Figure 8 shows the schematic permeation mechanism and CO, H_2, O_2, and CO_2 evolutions on both sides of this membrane reactor. From the feed side, two features must be noted: the presence of CO_2 and the absence of O_2. These results confirm that CO was oxidized to CO_2, at least partially, due to oxygen inverse permeation without realizing oxygen on the feed side. In fact, the maximum CO conversion was 18.4% at 900 °C. It must be noted that because oxygen was not supplied on the feed side, the CO oxidation was lower than that obtained in the first experiment (98.3%), in which O_2 was supplied on the feed side (see Figure 1).

This result confirms that oxygen inverse permeation is the limiting step of the entire reaction mechanism. In contrast, the sweep side results confirmed that only CO_2 was permeated because CO or H_2 were not detected. Although the membrane reactor gives a CO_2 flux of 1.08×10^{-3} mol/m^2 s because of a low CO_2 partial pressure, it can be observed that CO_2 recovery was improved from 36.1% to 64.6% by increasing temperature. In addition, a very important point to analyze is the possible H_2 oxidation. For example, if oxygen was released to the feed side, water would be produced, thus consuming hydrogen. Other possible H_2 consumption and water production processes could be produced by the reverse water gas shift (WGS) reaction. In such a case, CO concentration must be increased.

DOI: 10.1021/acsaem.8b01947
ACS Appl. Energy Mater. 2019, 2, 1380−1387

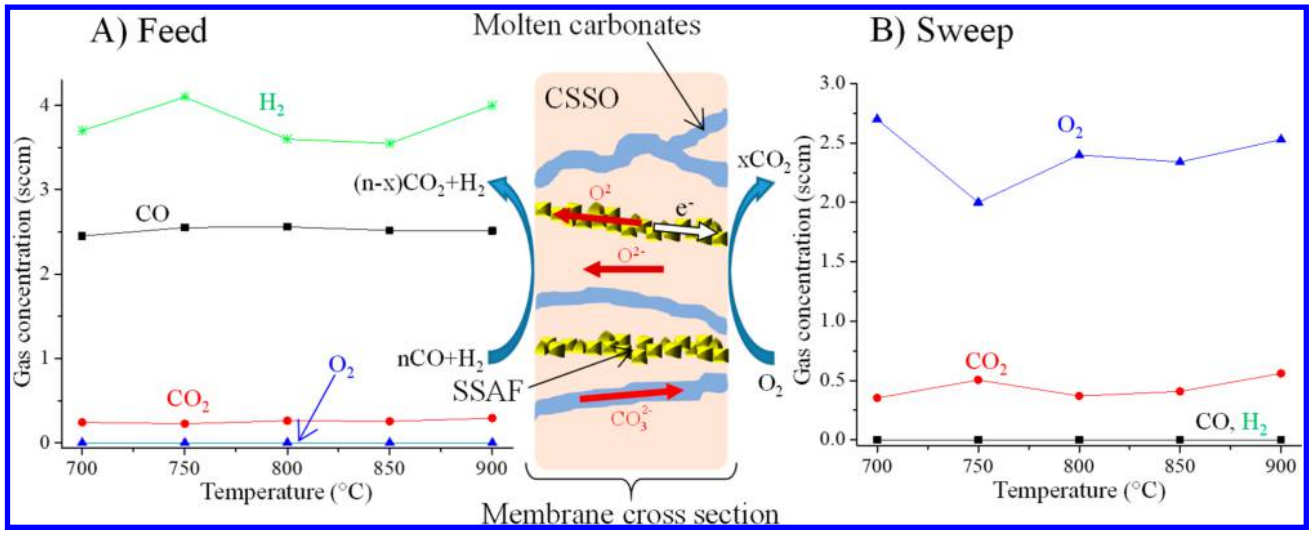

Figure 8. Schematic representation of CO oxidation and CO_2 permeation processes on a CSSO−SSAF−molten carbonate dense membrane reactor (center) and gas compositions on feed (A) and sweep (B) sides as a function of temperature.

To determine if water was produced, or not, the feed gas flow was further analyzed. Figure 9 shows the FTIR spectra and chromatograms of gas compositions on feed and sweep sides, as a function of temperature. In fact, these chromatograms (Figure 9A and 9B) were used to determine H_2, CO, CO_2, and O_2 concentrations on both sides of the membrane reactor, and they were already described above. Moreover, the CO_2 concentration evolutions are in good agreement with the thermal stability described above; where CO and CO_2 are partially sorbed at temperatures lower than 750 °C.

H_2O cannot be detected by using this gas chromatography column, thus FTIR was employed. FTIR spectra presented in Figure 9C compares the feed gas compositions at different temperatures. In addition, it is presented a FTIR spectrum containing specific amounts of $H_2O_{(v)}$, CO, and CO_2, diluted in argon, for comparison purposes. These FTIR spectra clearly evidence that $H_2O_{(v)}$ was produced, as water vapor vibration bands appeared between 4000 and 3400 cm^{-1}. However, water steam production efficiency should not be higher than 0.5 or 1.1 vol % at 700 and 900 °C, respectively. These values were estimated based on the semiquantitative calibration curves performed using different amounts of $H_2O_{(v)}$, CO_2 and CO. Moreover, the CO/H_2 oxidation selectivity (CO intensity/H_2 intensity of FTIR signals) of this membrane was estimated on around 39.1 at 700 °C and 19.4 at 900 °C, for the CO oxidation process.

These results show that CSSO−SSAF molten carbonate membrane reactor presented a low hydrogen oxidation level, which slightly increased as a function of temperature. On the other hand, CO oxidation was almost constant between 700 and 900 °C, although CO_2 permeation increased as a function of temperature. Therefore, CO oxidation was favored over steam formation because of CO adsorption affinity related to acid−base site of attraction, as well as on catalytic properties and different oxidation enthalpies (see reactions 1 and 2).

These results confirm a positive effect of SSAF on this membrane reactor due to oxygen inverse permeation, potentiating CO oxidation and CO_3^{2-} formation processes, while hydrogen oxidation is not so high. Therefore, this kind of membrane reactor systems seems to operate as follows. Initially, O_2 is fed and dissociated on the sweep side (reaction 5), producing O^{2-} anions. These anions permeate from the sweep to the feed side, mainly through the SSAF phase. Once O^{2-} anions arrive to the feed side, a portion of them react with CO (producing CO_2, reaction 6), while others produce CO_3^{2-} (reaction 7). Finally, carbonates and electrons move back to the sweep side through the molten carbonates and SSAF phases, respectively. Stoichiometrically, according to this mechanism in which CO_2 is the final permeated species, only half of the O^{2-} formed on the sweep side is recovered after the entire process (those used in carbonate formation, inverse reaction 7), while the other half oxygen anions are consumed during CO oxidation.

$$O_2 + 4e^- \leftrightarrow 2O^{2-} \quad (5)$$

$$CO + O^{2-} \leftrightarrow CO_2 + 2e^- \quad (6)$$

$$CO_2 + O^{2-} \leftrightarrow CO_3^{2-} \quad (7)$$

In summary, this kind of membrane reactor can permeate CO as CO_2 from syngas mixtures without almost affecting the H_2 content. Thus, H_2 can be enriched, although hydrogen oxidation must be eliminated. On the opposite membrane reactor side, a mixture of recovered CO_2 and O_2 is formed, unless all oxygen is permeated and consumed on the reaction side. These two final flow compositions are useful in different hydrogen purification and syngas combustion-assisted CO_2 capture system designs.[30]

■ CONCLUSIONS

The CSSO−SSAF system was successfully tested as a new possible dense ceramic-carbonate membrane reactor for CO oxidation and subsequent CO_2 permeation. Both processes were initially tested on a CSSO-molten carbonate membrane reactor, with CO and O_2 feeding on the oxidation reaction side, presenting CO oxidation efficiencies as high as 98.3%. After this initial test, different gas compositions were evaluated, probing that CSSO membrane reactor is able to act as an active phase, during CO oxidation and as a permeation system. However, this gas mixture would not be used in real systems because of the presence of hydrogen and its possible oxidation. Then, a different molten carbonate membrane reactor was prepared and an oxygen inverse permeation was proposed by

DOI: 10.1021/acsaem.8b01947
ACS Appl. Energy Mater. 2019, 2, 1380−1387

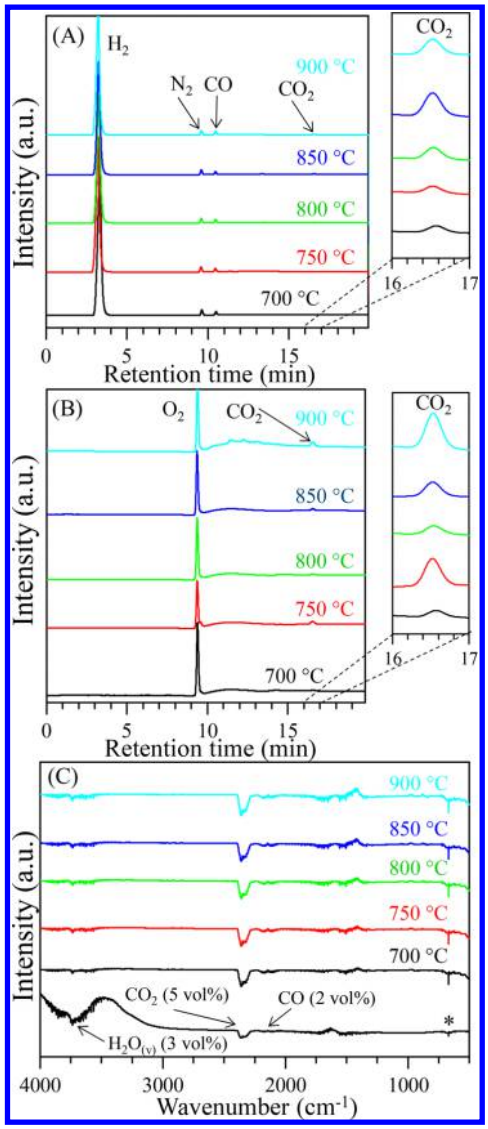

Figure 9. Gas chromatograms of feed (A) and sweep (B) sides and FTIR spectra of feed side (C) for the CSSO−SSAF−molten carbonate dense membrane reactor at different temperatures. On the FTIR spectra, it was included a FTIR spectrum ($H_2O_{(v)}$, CO, and CO_2 gas mixture diluted in Ar, labeled as *) used for determining semiquantitatively the $H_2O_{(v)}$ concentration for comparison purposes.

feeding O_2 on the sweep side. The ceramic-molten carbonate dense membrane reactor was prepared with CSSO and inclusion of a good oxygen conductor (SSAF), which promotes electron conduction and oxygen inverse permeation. The results show that oxygen inverse permeation improves CO oxidation and CO_3^{2-} formation, which subsequently diffuse on the molten carbonate phase and they are finally released as CO_2 on the sweep side, while H_2 is almost not affected (oxidized) on the feed side. Of course, more and deeper studies have to be perform to increase the CO oxidation-permeation, inhibiting any hydrogen oxidation.

AUTHOR INFORMATION

Corresponding Author

*Phone: +52 (55) 5622 4627. E-mail: pfeiffer@materiales.unam.mx.

ORCID

Oscar Ovalle-Encinia: 0000-0002-1394-2676

Heriberto Pfeiffer: 0000-0002-6217-3420

Notes

The authors declare no competing financial interest.

ACKNOWLEDGMENTS

This work was financially supported by project SENER-CONACYT (251801). Authors thank to J. E. Romero-Ibarra for technical assistance.

REFERENCES

(1) Olajire, A. A. CO_2 capture and separation technologies for end-of-pipe applications—A review. *Energy* **2010**, *35*, 2610−2628.

(2) Deng, L.; Hägg, M. B. Fabrication and evaluation of a blend facilitated transport membrane for CO_2/CH_4 separation. *Ind. Eng. Chem. Res.* **2015**, *54*, 11139−11150.

(3) Franz, J.; Scherer, V. An evaluation of CO_2 and H_2 selective polymeric membranes for CO_2 separation in IGCC processes. *J. Membr. Sci.* **2010**, *359*, 173−183.

(4) Korelskiy, D.; Ye, P.; Fouladvand, S.; Karimi, S.; Sjöberg, E.; Hedlund, J. Efficient ceramic zeolite membranes for CO_2/H_2 separation. *J. Mater. Chem. A* **2015**, *3*, 12500−12506.

(5) Chen, Y.; Liao, Q.; Li, Z.; Wang, H.; Wei, Y.; Feldhoff, A.; Caro, J. A CO_2-stable hollow-fiber membrane with high hydrogen permeation flux. *AIChE J.* **2015**, *61*, 1997−2007.

(6) Hibino, T.; Kobayashi, K.; Ito, M.; Ma, Q.; Nagao, M.; Fukui, M.; Teranishi, S. Efficient hydrogen production by direct electrolysis of waste biomass at intermediate temperatures. *ACS Sustainable Chem. Eng.* **2018**, *6*, 9360−9368.

(7) Yacou, C.; Smart, S.; Diniz da Costa, J. C. Long term performance cobalt oxide silica membrane module for high temperature H_2 separation. *Energy Environ. Sci.* **2012**, *5*, 5820−5832.

(8) Dai, Z.; Ansaloni, L.; Deng, L. Precombustion CO_2 capture in polymeric hollow fiber membrane contactors using ionic liquids: Porous membrane versus nonporous composite membrane. *Ind. Eng. Chem. Res.* **2016**, *55*, 5983−5992.

(9) Bux, H.; Feldhoff, A.; Cravillon, J.; Wiebcke, M.; Li, Y.-S.; Caro, J. Oriented zeolitic imidazolate framework-8 membrane with sharp H_2/C_3H_8 molecular sieve separation. *Chem. Mater.* **2011**, *23*, 2262−2269.

(10) Hwang, S. Y.; Zhang, C.; Yurchekfrodl, E.; Peng, Z. Property of Pt−Ag alloy nanoparticle catalysts in carbon monoxide oxidation. *J. Phys. Chem. C* **2014**, *118*, 28739−28745.

(11) Zhao, W.; Bai, J.; Francisco, J. S.; Zeng, X. C. Formation of CO_2 hydrates within single-walled carbon nanotubes at ambient pressure: CO_2 capture and selective separation of a CO_2/H_2 mixture in water. *J. Phys. Chem. C* **2018**, *122*, 7951−7958.

(12) Chen, B.; Ruan, X.; Jiang, X.; Xiao, W.; He, G. Dual-membrane module and its optimal flow pattern for H_2/CO_2 separation. *Ind. Eng. Chem. Res.* **2016**, *55*, 1064−1075.

(13) Tao, Y.; Xue, Q.; Liu, Z.; Shan, M.; Ling, C.; Wu, T.; Li, X. Tunable hydrogen separation in porous graphene membrane: First-principle and molecular dynamic simulation. *ACS Appl. Mater. Interfaces* **2014**, *6*, 8048−8058.

(14) Navlani-García, M.; Miguel-García, I.; Berenguer-Murcia, A.; Lozano-Castelló, D.; Cazorla-Amorós, D.; Yamashita, H. Pd/zeolite-based catalysts for the preferential CO oxidation reaction: ion-exchange, Si/Al and structure effect. *Catal. Sci. Technol.* **2016**, *6*, 2623−2632.

(15) Alves, H. J.; Bley, C., Jr.; Niklevicz, R. R.; Frigo, E. P.; Frigo, M. S.; Coimbra-Araújo, C. H. Overview of hydrogen production technologies from biogas and the applications in fuel cells. *Int. J. Hydrogen Energy* **2013**, *38*, 5215−5225.

(16) Ke, X. B.; Zhu, H. Y.; Gao, H. Y.; Liu, J. W.; Zheng, Z. F. High-performance ceramic membranes with a separation layer of metal oxide nanofibers. *Adv. Mater.* **2007**, *19*, 785−790.

DOI: 10.1021/acsaem.8b01947
ACS Appl. Energy Mater. 2019, 2, 1380−1387

(17) Das, J. K.; Das, N. Mercaptoundecanoic acid capped palladium nanoparticles in a SAPO 34 membrane: a solution for enhancement of H_2/CO_2 separation efficiency. *ACS Appl. Mater. Interfaces* **2014**, *6*, 20717−20728.
(18) Chung, S. J.; Park, J. H.; Li, D.; Ida, J. I.; Kumakiri, I.; Lin, Y. S. Dual-phase metal−carbonate membrane for high-temperature carbon dioxide separation. *Ind. Eng. Chem. Res.* **2005**, *44*, 7999−8006.
(19) Wade, J. L.; Lee, C.; West, A. C.; Lackner, K. S. Composite electrolyte membranes for high temperature CO_2 separation. *J. Membr. Sci.* **2011**, *369*, 20−29.
(20) Ovalle-Encinia, O.; Pfeiffer, H.; Ortiz-Landeros, J. $Ce_{0.85}Sm_{0.15}O_2$-$Sm_{0.6}Sr_{0.4}Al_{0.3}Fe_{0.7}O_3$ composite for the preparation of dense ceramic-carbonate membranes for CO_2 separation. *J. Membr. Sci.* **2018**, *547*, 11−18.
(21) Zhang, L.; Xu, N.; Li, X.; Wang, S.; Huang, K.; Harris, W. H.; Chiu, W. K. S. High CO_2 permeation flux enabled by highly interconnected three-dimensional ionic channels in selective CO_2 separation membranes. *Energy Environ. Sci.* **2012**, *5*, 8310−8317.
(22) Norton, T. T.; Ortiz-Landeros, J.; Lin, Y. S. Stability of La−Sr−Co−Fe oxide−carbonate dual-phase membranes for carbon dioxide separation at high temperatures. *Ind. Eng. Chem. Res.* **2014**, *53*, 2432−2440.
(23) Anderson, M.; Lin, Y. S. Carbonate−ceramic dual-phase membrane for carbon dioxide separation. *J. Membr. Sci.* **2010**, *357*, 122−129.
(24) Zhu, X.; Liu, Y.; Cong, Y.; Yang, W. $Ce_{0.85}Sm_{0.15}O_{1.925}$−$Sm_{0.6}Sr_{0.4}Al_{0.3}Fe_{0.7}O_3$ dual-phase membranes: one-pot synthesis and stability in a CO_2 atmosphere. *Solid State Ionics* **2013**, *253*, 57−63.
(25) Dong, X.; Lin, Y. S. Catalyst-free ceramic-carbonate dual phase membrane reactor for hydrogen production from gasifier syngas. *J. Membr. Sci.* **2016**, *520*, 907−913.
(26) Thursfield, A.; Murugan, A.; Franca, R.; Metcalfe, I. S. Chemical looping and oxygen permeable ceramic membranes for hydrogen production−a review. *Energy Environ. Sci.* **2012**, *5*, 7421−7459.
(27) Reina, T. R.; Papadopoulou, E.; Palma, S.; Ivanova, S.; Centeno, M. A.; Ioannides, T.; Odriozola, J. A. Could an efficient WGS catalyst be useful in the CO-PrO_x reaction? *Appl. Catal., B* **2014**, *150−151*, 554−563.
(28) Zhu, X.; Wang, H.; Yang, W. Relationship between homogeneity and oxygen permeability of composite membranes. *J. Membr. Sci.* **2008**, *309*, 120−127.
(29) Ovalle-Encinia, O.; Mendoza-Nieto, J. A.; Ortiz-Landeros, J.; Pfeiffer, H. $Ce_{0.8}Sm_{0.15}Sr_{0.05}O_2$ as possible oxidation catalyst and assessment of the CaO addition in the coupled CO oxidation−CO_2 capture process. *Ind. Eng. Chem. Res.* **2017**, *56*, 6124−6130.
(30) Sherman, S. R.; Gray, J. R.; Brinkman, K. S.; Huang, K. Combustion-assisted CO_2 capture using MECC membranes. *J. Membr. Sci.* **2012**, *401−402*, 323−332.

DOI: 10.1021/acsaem.8b01947
ACS Appl. Energy Mater. 2019, 2, 1380−1387